Advanced charge injection devices for space instruments

Kyle Miller and Kathy Doughty,
Mission Research Corporation, 5017 N. 30th Street, Colorado Springs, CO, USA 80919

ABSTRACT

Charge Injection Devices (CIDs) have historically played a niche role in visible imager technologies, mainly for applications requiring high radiation tolerance. They have not exhibited the radiometric performance of competing visible- imaging technologies such as CCDs, and so have not been widely applied to space instrument systems. Recent advances in CIDs have demonstrated much higher radiometric performance as well as lower noise operation, without compromising the radiation tolerance of the devices, making the devices suitable for a wide range of space instruments. We present radiometric, noise, and radiation response data for several of the newest CID designs that are candidate technologies for visible space telescope systems.

1. INTRODUCTION

Charge injection devices (CIDs) were developed at approximately the same time as the nearly -ubiquitous charge-coupled device (CCD), but have not received the same acceptance in the scientific imaging community. This is primarily due to the higher read noise inherent in the design in which the output amplifier must "see" the capacitance of the entire device, whereas the CCD has a very low read noise due to a small readout capacitor. However, CID's have also historically demonstrated a vast superiority to the CCD in radiation tolerance, with some designs demonstrating capabilities in the mega-rad range. CCDs are well known to be susceptible to both ionizing and non-ionizing radiation damage, which can limit their performance in a space-based application by dramatically decreasing the charge transfer efficiency whereby charge is moved from one pixel to the next.

We discuss a new development in CID technology which focuses on devices that can be used in a stellar reference unit (star tracker). This development effort was initiated by the Jet Propulsion Laboratory, under the Europa Orbiter program, who which demonstrated a need for a highly radiation- tolerant imager that could withstand the high-energy electron environment around Jupiter. The high-energy electron environment produces lifetime damage effects (total ionizing dose and silicon displacement damage effects) as well transient noise generated caused by the high-energy electrons impinging on the pixel storage units and generating spurious signal. The device is also designed needed to meet the radiometric requirements for use in a moderately accurate star tracker. Two devices were developed as a result of this program: the CID816, which features a preamplifier-per-row design and the CID817, which is a preamplifier-per-pixel design. In addition, a third device is under development (delivered wafers) which is a preamplifier-per-pixel design that is thinned and backside illuminated. The thinning is done to reduce the per-charged-particle noise on the detector by reducing the volume of active material that charged particles can interact with, and Backside thinning illumination is used to increase the fill factor and effective device responsivity.

The CID816s have been available for approximately 9 months, and have been had preliminary radiometric characterization performed as well as some radiation characterization. The CID817 and CID818 are recent developments and are still in fabrication. Radiation and radiometric characterization is due to occur during the fall of 2003.

2. CID OPERATION

The basic CID operation has been described before[1234] and the new imagers follow the same basic concepts. The CID pixel structure utilizes two overlapping MOS capacitors and senses the charge transfer between the two storage sites. The output can be sensed by an amplifier on each device, amplifiers in the row or column, or by in-pixel

amplifiers. Because the readout mechanism is non-destructive, i.e., the charge is not removed during a readout cycle, the temporal noise can be reduced by averaging multiple reads of the same charge and averaging. This feature also allows multiple frame integration which creates the ability for differing dynamic ranges across the imager. The pre-amplifier per pixel design allows random addressing of individual pixels or windows without reading out the entire imager, allowing for unique scientific applications to be designed. Figure 1 shows the basic pixel operation of the devices.

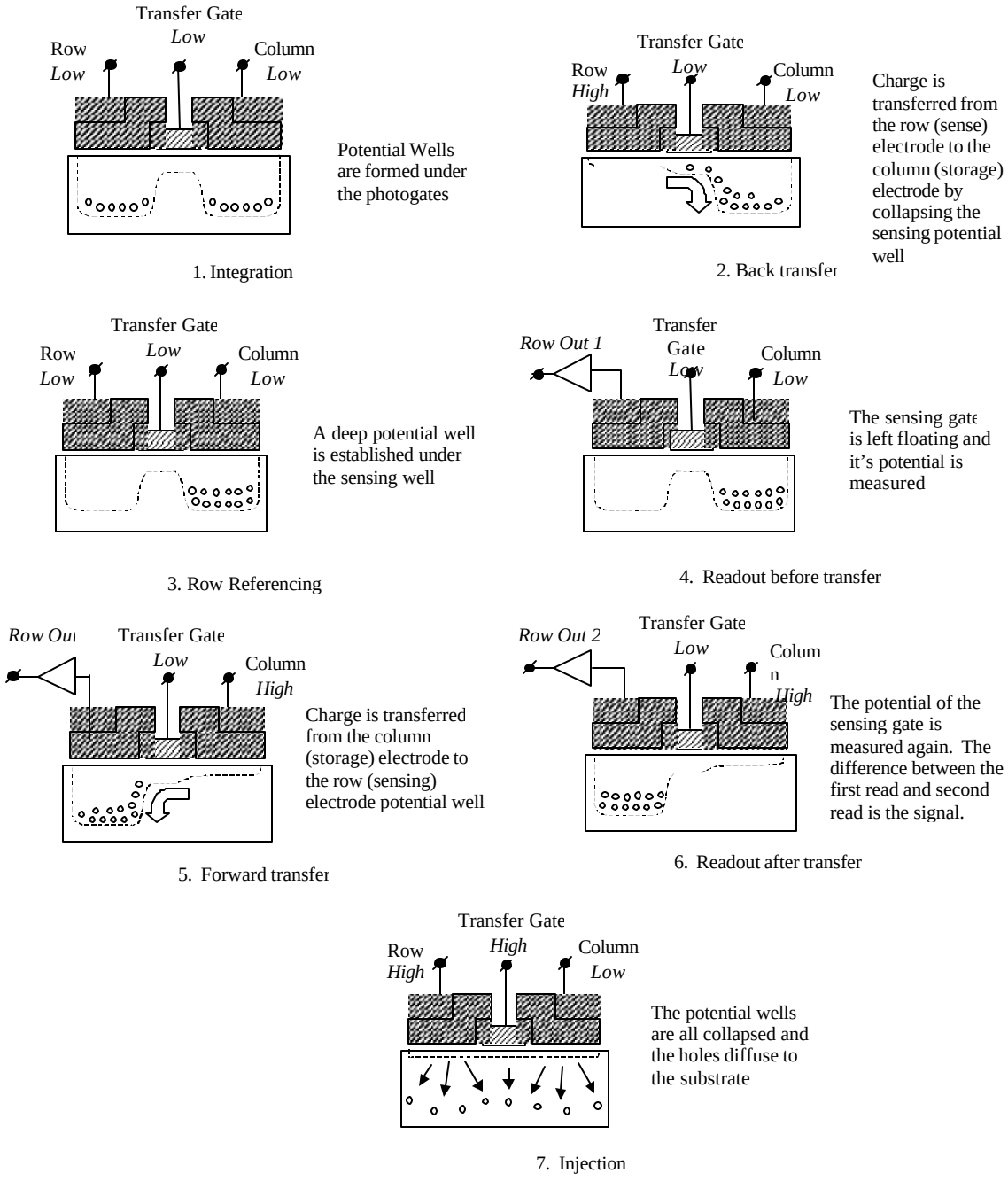

Figure 1: CID Operation

3. CID DESCRIPTIONS

Descriptions of the three devices are shown in the following table:

Device Parameter	**CID816**	**CID817**	**CID818**
Substrate Material	n+ epi on p silicon	n+ epi on p silicon	n+ epi on p silicon
Architecture	All PMOS	All PMOS	All PMOS
Pixels	512 x 512	512 x 512	512 x 512
Pixel Pitch	27 micron square	27 micron square	27 micron square
Amplifier	Pre-amp per row	Pre-amp per pixel	Pre-amp per pixel
Random Access	Yes	Yes	Yes
Thinned	No	No	Yes (nominal 7 microns)
Backside Illuminated	No	No	Yes
Device Design Goal Specifications			
Read Noise	< 200 electrons at 50 kHz	< 50 electron/pixel @ 50 kHz	< 50 electron/pixel @ 50 kHz
Linearity	< 2% pixel capacity	< 2% pixel capacity	< 2% pixel capacity
Bright row defects	0	0	0
Bright column defects	0	0	0
Cold Pixels	< 16	< 16	<16
Dark fixed pattern noise	< 100 electrons	< 100 electrons	< 100 electrons
Mean dark current	< 0.025 nA/cm2	< 0.025 nA/cm2	< 0.025 nA/cm2
Threshold Shift (in radiation)	-5 mV/krad(Si)	-5 mV/krad(Si)	-5 mV/krad(Si)

4. RADIOMETRIC DATA

Radiometric and noise data was taken for a number of CID816 imagers. Figure 2 shows the measured quantum efficiency for four devices along with the mean measured for a total of 10 devices. Figure 3 shows the mean per-pixel read noise measured at -40C to eliminate contributions from dark current for 10 different devices. Figure 4 shows the mean per-pixel dark current for the same 10 devices measured at -20C, 0C, and +20C. Figure 5 shows the full-well capacity of the same 10 devices.

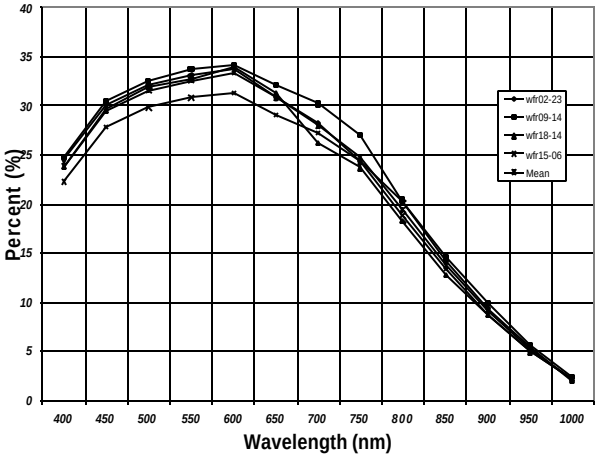

Figure 2: CID816 Quantum Efficiency

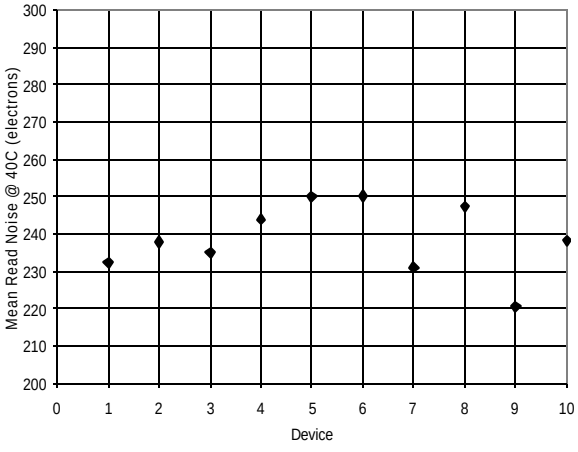

Figure 3: CID816 Mean Read Noise

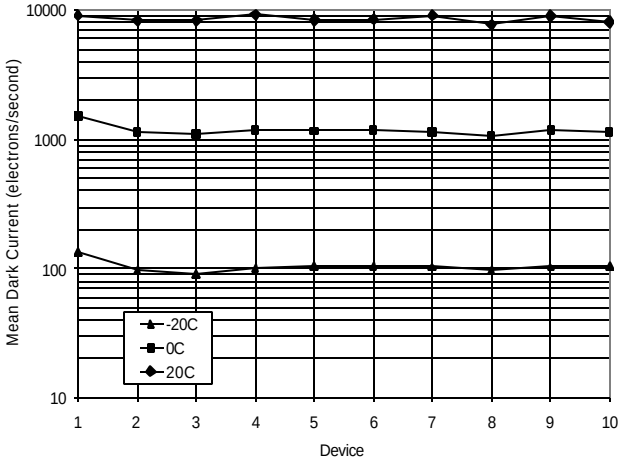

Figure 4: CID816 Mean Dark Current

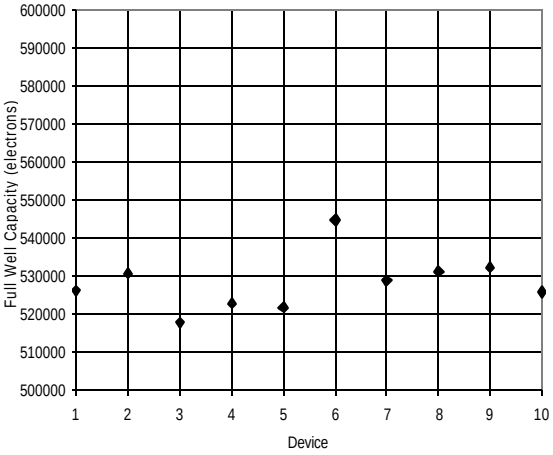

Figure 5: CID816 Full Well Capacity

5. RADIATION DATA

Proton Testing was performed at the Crocker Nuclear Laboratory, University of California, Davis. Protons of 45 MeV and 63 MeV were used which, when translated through the window of the enclosing dewar, correspond to approximately 17 and 60 MeV protons at the device. Two effects were measured: the device noise characteristics as a function of total proton fluence, and the transient noise effects due to the proton flux.

5.1 TOTAL PROTON FLUENCE CHARACTERIZATION

Noise characteristics for the device were taken from 0 to 50Krads. Above 50Krads the variation between the per-column amplifiers' radiation compensation set-points became large enough that the columns could not be brought simultaneously into range. Work on addressing this issue though setting of epi-layer voltage is underway.

5.1.1 MEAN READ NOISE

Mean Read Noise is a measure of the frame-to-frame temporal variation of any individual pixel value. The test is run with no light on the device. The temperature was held at a relatively cold value of -30C to eliminate dark current contribution. Data was measured on 10 full imager frames (512x512 pixels). Mean Read Noise remained fairly constant at 300-400 e-/read as shown in Figure 6.

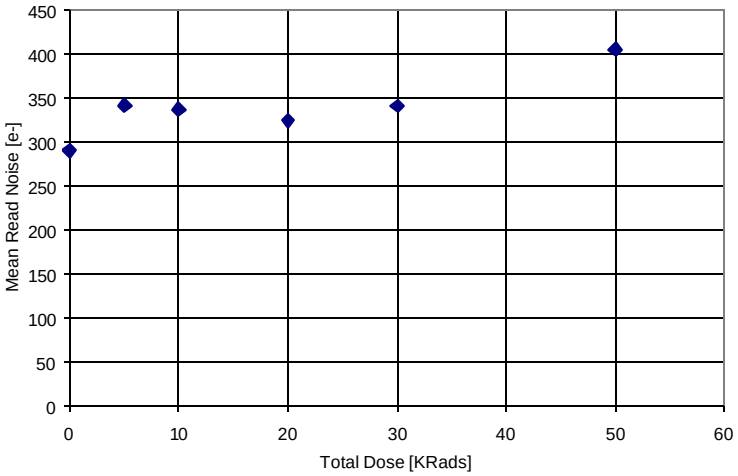

Figure 6: Mean Read Noise as a function of total proton dose

5.1.2 READ FIXED PATTERN NOISE (RFPN)

RFPN is a measurement of the spatial variation of read noise measured across all pixels. Again, the data was taken with no incident optical signal, and was measured at –30C to eliminate dark current contribution. Data was measured on 10 full imager frames (512x512 pixels). There was a definite increase in RFPN with dose as shown in Figure 7, although this is probably largely due to variation in amplifier set-point, as shown in Figure 7.

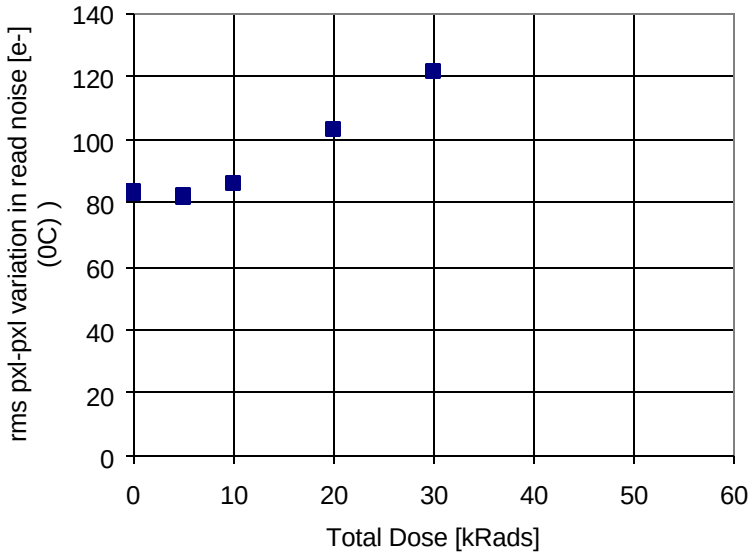

Figure 7: Read Fixed Pattern Noise

5.1.3 LINEARITY

Linearity is shown as the standard deviation of the signal at 2/3 well-fill. The initial values were under 5%, increasing with total fluence. Again, column-to-column variation accounts for the bulk of the increase.

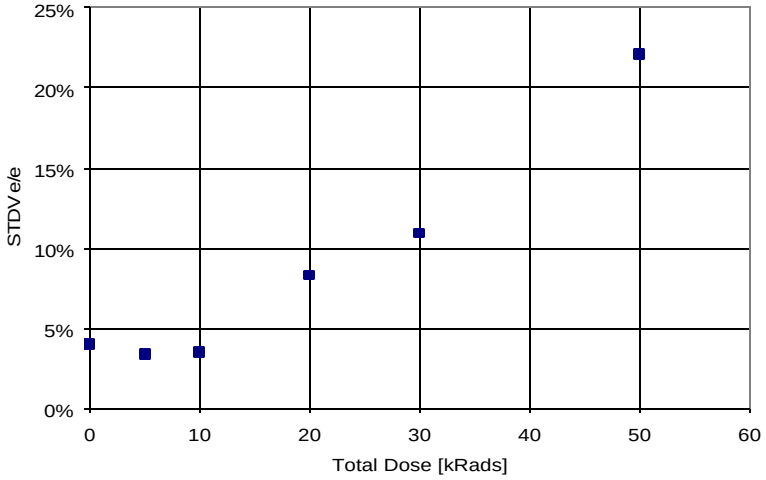

Figure 8: Linearity as function of total proton fluence

5.2 TRANSIENT PROTON RADIATION RESPONSE

The response of the device to proton transients was also measured as a part of the characterization procedure. As protons travel through the device, electron/hole pairs are generated that are indistinguishable from those created by photon absorption. This introduces a noise source that is dependent on the proton flux. To measure this, data was taken in no-light conditions under a constant proton flux. Full-frame data was read out column by column. Because the columns were read off sequentially, the amount of time a column was exposed to the radiation flux depended on where that column was in the read-out order. This method therefore generated a series of data points in which the column-to-column difference depends on the proton flux times the column read-out time. Example data is shown in Figure 9. A fit is made to the linear region of response. Taking into account the proton flux and column read-out time gave a mean per-proton signal of 7500 e-/proton for the 17 MeV protons and 5200 e-/proton for the 60 MeV protons. In a device, this transient radiation response would contribute an additional per-pixel noise of

$$\sqrt{2 \cdot N} \cdot PH$$

Where N is the number of radiation events/pixel/frame and PH is the mean per-proton signal. These values are expected to drop markedly for the thinner devices (CID 818).

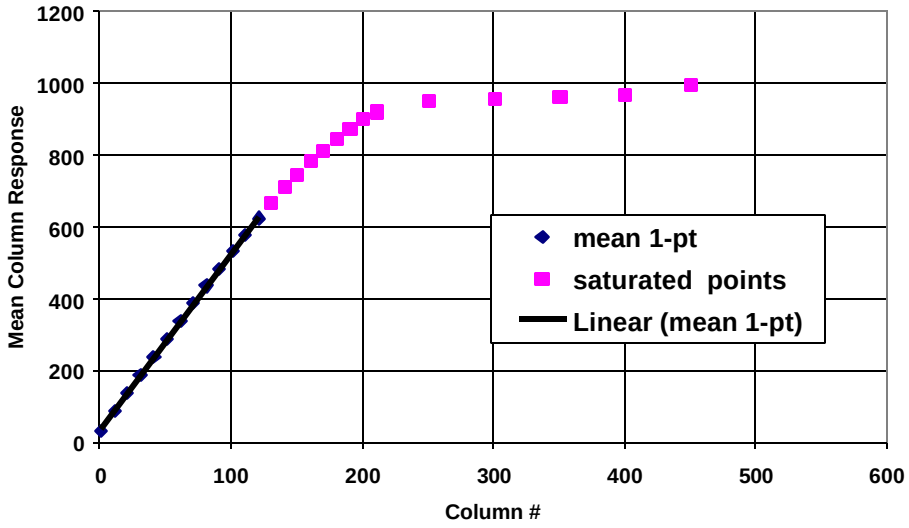

Figure 9: Mean column response for 17 MeV protons

6. CONCLUSIONS

The new CID imagers entering the market show considerable improvement over previous versions. Present amplifier-per-column devices (CID816s) show a measured noise floor of around 250 electrons, with a factor of 5 or better expected for the amplifier-per-pixel devices currently in production. The CID816s show a 30 to 35% peak QE, with a ½ million electron full-well. Back-side illumination of the CID818s is expected to increase the QE to 80% or above. The measured values hold out to 50Krads Total Dose, and the tolerable dose is expected to rise sharply with adjustments to the compensation circuits. The transient response to radiation is consistent with that expected for the active region size, and is similar to that seen for other unthinned devices of other types (e.g.: CCDs, APSs, hybridized PN junctions). Thinning the devices will reduce this value by a factor of 2 or more. These results indicate that the emerging CID devices will not only be radiation tolerant but also demonstrate radiometric performance that will enable them to compete in the visible space instrument market.

REFERENCES

[1] Zarnowski, J., et. al., "Selectable One to Four Port, Very High Speed 512 x 512 Charge Injection Device", Proc. SPIE, Vol. 1447, pg. 191-201, 1991.
[2] Wentink, R., et. al., "CID Detectors for X-Ray Imaging", SPIE, San Diego, 1994.
[3] Carbone, J., et. al., "Application of Low Noise CID Imagers in Scientific Instrumentation Cameras", SPIE Vol. 1447, Feb 25-27,1991, pg. 229-242.
[4] J. Carbone, et. al., "Megarad and Scientific CIDs", SPIE IS&TS Symposium on Electronic Imaging and Technology, 1996.